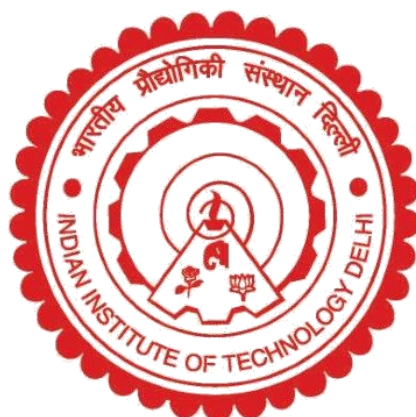


CHEMICAL SENSING USING THZ TIME- DOMAIN SPECTROSCOPY

KHUSHBOO SINGH



**DEPARTMENT OF PHYSICS
INDIAN INSTITUTE OF TECHNOLOGY DELHI
DECEMBER 2022**

©Indian Institute of Technology Delhi (IITD), New Delhi, 2022

CHEMICAL SENSING USING THZ TIME-DOMAIN SPECTROSCOPY

by

KHUSHBOO SINGH

Department of Physics

Submitted

*in the fulfillment of requirements of the degree of **Doctor of
Philosophy** to the*



INDIAN INSTITUTE OF TECHNOLOGY DELHI
DECEMBER 2022


Dedicated to my brother Prashant

Certificate

This is to certify that the dissertation titled “**Chemical sensing using Terahertz time-domain spectroscopy**”, being submitted by **Khushboo Singh** to the Indian Institute of Technology Delhi, for the award of the degree of **Doctor of Philosophy**, is a record of bonafide research work carried out by her. She has worked under my guidance and supervision and has fulfilled the requirements, which to my knowledge, have reached the requisite standard for the submission of this dissertation. The results contained in this dissertation have not been submitted in part or full to any other University or Institute for the award of any degree or diploma.

Date: Dec 21, 2022

Place: New Delhi

 Digitally signed by
Amartya Sengupta
Date: 2022.12.21
12:14:11 +05'30'

Prof. Amartya Sengupta

Department of Physics

Indian Institute of Technology Delhi

New Delhi, India

Acknowledgements

First and foremost, I would like to express my profound gratitude to my supervisor, Prof. Amartya Sengupta, for introducing me to the fascinating world of optics and optical spectroscopy. I am grateful for his scholarly guidance, patience and support which helped me explore different facets of my research problem and encouraged me to perform challenging and enthusiastic research studies. I would also like to thank Dr Aparajita Bandyopadhyay for her invaluable time, long enriching technical discussions, and for sharing her technical expertise in the frontier of terahertz technology.

Besides my supervisor, I would like to thank my research committee members, Prof. M. R. Shenoy, Prof. Sunil Kumar, and Prof. Pramit Chowdhury, for their insightful comments, feedback, and suggestions for the betterment of my research work. I would also like to give special thanks to Prof. Aleksandar Rakic, University of Queensland, for giving me the opportunity to work on the complementary experimental set-ups in his laboratory for the rigorous study of my research work.

I am extremely thankful to my friends and colleagues, especially, my first lab partner - Diksha Garg, my roommates - Preeti Sharma and Shivani Sharma and teammates - Uzair Aalam, Urbi Kundu and Mayuri Kashyap, for always being there to support me throughout this magnificent and challenging journey.

I would like to thank my friend Rishi, for his unconditional support and care through this venture. It is impossible to extend enough thanks to my family, especially, my parents, sister, brother, brother-in-law and my little nephews, Aaryaman and Aanjanya, for empowering me and always believing in me no matter what. They always inspired me to be a better person and this dissertation is a testament of their patience and understanding.

Khushboo Singh

Abstract

The terahertz frequency range, sandwiched between the electronic microwave range and photonic infrared range, exhibits several unique features that have been of great scientific interest for several decades. This portion of the electromagnetic wave ranges from 0.1 – 10 THz. Owing to the unique attributes of terahertz radiations and the technological advancements in the field of ultrafast optics, terahertz spectroscopy has emerged as a non-destructive technique for numerous applications such as biomedical diagnostics, material characterization, security screening, astronomy, agri-food and process control in industries. Most of these applications are directly or indirectly related to selective sensing of chemicals and biochemicals.

In this dissertation entitled “Chemical sensing using terahertz time-domain spectroscopy”, we have employed terahertz spectroscopy and imaging techniques to study the optical response of a large variety of chemicals towards implementation in precision agriculture, industrial process control and material characterization. Different classes of chemicals investigated in this dissertation include biochemicals such as water and plant pigments (chlorophyll, carotenoid, betalain and anthocyanin) for precision agriculture application; common organic compounds such as aromatic nitro-compounds and their derivatives, solid polymer composites systems (binary, ternary and quaternary), pharmaceuticals and genetically modified plants.

The major thrust of this dissertation is the development of improved methodologies to overcome the experimental challenges, thereby demonstrating the possibility of the successful implementation of terahertz spectroscopy and imaging techniques for sensing purposes in several agri-photonics applications. We have demonstrated the application of quantum cascade laser-based laser feedback interferometry imaging technique for hydration mapping in plants and compared its feasibility and viability with the photoconductive antenna based broadband terahertz imaging towards field deployability. Additionally, the dissertation focuses on the

utilization of suitable theoretical models and signal processing tools to address the existing challenges such as dispersion in granular composites and false quality assessment of complex composite systems, such as pharmaceuticals, where a multi-variate analysis is required for accurate quality assessment and management.

सार

टेराहर्ट्ज़ आवृत्ति पट्ट, इलेक्ट्रॉनिक माइक्रोवेव पट्ट और फोटोनिक इन्फ्रारेड पट्ट के बीच, कई अनूठी विशेषताओं को प्रदर्शित करता है जो कई दशकों से महान वैज्ञानिक रुचि का रहा है। विद्युत चुम्बकीय तरंग का यह भाग 0.1 - 10 THz तक होता है। टेराहर्ट्ज़ विकिरणों की अनूठी विशेषताओं और अल्ट्राफास्ट ऑप्टिक्स के क्षेत्र में तकनीकी प्रगति के कारण, टेराहर्ट्ज़ स्पेक्ट्रोस्कोपी बायोमेडिकल डायग्नोस्टिक्स, सामग्री लक्षण वर्णन, सुरक्षा स्क्रीनिंग, खगोल विज्ञान, उद्योगों में नियंत्रण, कृषि-खाद्य और प्रक्रिया जैसे कई अनुप्रयोगों के लिए एक गैर-विनाशकारी तकनीक के रूप में उभरा है। इनमें से अधिकांश अनुप्रयोग प्रत्यक्ष या अप्रत्यक्ष रूप से रसायनों और जैव रसायनों के चयनात्मक संवेदन से संबंधित हैं।

"टेराहर्ट्ज़ टाइम-डोमेन स्पेक्ट्रोस्कोपी का उपयोग करते हुए रासायनिक संवेदन" शीर्षक वाले इस शोध प्रबंध में, हमने सटीक कृषि, औद्योगिक प्रक्रिया नियंत्रण और सामग्री लक्षण वर्णन में कार्यान्वयन के लिए रसायनों की एक विशाल विविधता की ऑप्टिकल प्रतिक्रिया का अध्ययन करने के लिए टेराहर्ट्ज़ स्पेक्ट्रोस्कोपी और इमेजिंग तकनीकों को नियोजित किया है। इस शोध प्रबंध में जांच किए गए रसायनों के विभिन्न वर्गों में सटीक कृषि अनुप्रयोग के लिए जैव रसायन जैसे पानी और पौधों के वर्णक (क्लोरोफिल, कैरोटीनॉयड, बीटालाइन और एंथोसायनिन) शामिल हैं; आम कार्बनिक यौगिक जैसे सुगंधित नाइट्रो-यौगिक और उनके डेरिवेटिव, ठोस बहुलक कंपोजिट सिस्टम (बाइनरी, टर्नरी और क्वाटर्नरी), फार्मास्यूटिकल्स और आनुवंशिक रूप से संशोधित पौधे।

इस शोध प्रबंध का प्रमुख जोर प्रयोगात्मक चुनौतियों से निपटने के लिए उन्नत पद्धतियों का विकास है, जिससे कई कृषि-फोटोनिक्स अनुप्रयोगों में सेंसिंग उद्देश्यों के लिए टेराहर्ट्ज़ स्पेक्ट्रोस्कोपी और इमेजिंग तकनीकों के सफल कार्यान्वयन की संभावना प्रदर्शित होती है। हमने पौधों में हाइड्रेशन मैपिंग के लिए क्वांटम कैस्केड लेजर-आधारित लेजर फीडबैक इंटरफेरोमेट्री इमेजिंग तकनीक के अनुप्रयोग का प्रदर्शन

किया है और इसकी व्यवहार्यता और व्यवहार्यता की तुलना फील्ड डिप्लॉयबिलिटी की दिशा में फोटोकंडक्टिव एंटीना आधारित ब्रॉडबैंड टेराहर्ट्ज़ इमेजिंग से की है। इसके अतिरिक्त, शोध प्रबंध उपयुक्त सैद्धांतिक मॉडल और सिग्नल प्रोसेसिंग टूल के उपयोग पर ध्यान केंद्रित करता है ताकि मौजूदा चुनौतियों का समाधान किया जा सके जैसे कि दानेदार कंपोजिट में फैलाव और जटिल कंपोजिट सिस्टम का गलत गुणवत्ता मूल्यांकन, जैसे कि फार्मास्यूटिकल्स, जहां सटीक गुणवत्ता मूल्यांकन और प्रबंधन के लिए एक बहु-चर विश्लेषण आवश्यक है ।

Table of Contents

Certificate	i
Acknowledgement	ii
Abstract.....	v
Table of content.....	ix
List of figures.....	xiii
List of tables.....	xxiii
List of abbreviations	xxiv
1. Introduction.....	1
1.1. Background of terahertz technology	1
1.2. Attributes of THz radiation	2
1.3. Motivation	6
1.4. Dissertation overview	9
1.5. Original contribution of the dissertation	12
2. Instrumentation and techniques in THz range	14
2.1. Introduction to THz sources	14
2.1.1. THz sources based on vacuum electronics	15
2.1.2. Laser sources	17
2.1.3. Optical rectification	21
2.1.4. Photoconductive switch	21
2.2. Introduction to THz detectors	24

4.4.Result and discussion	70
4.4.1. Aromatic nitro-compounds	70
4.4.2. Derivatives of benzoic acids	74
4.4.3. Acid salt: KNO ₃	77
4.4.4. Nitroimine: NQ	78
4.4.5. Amide:Urea.....	79
4.5.Conclusion	81
5. Optical parameter extraction of composites with different types of fillers using THz-TDS and effective medium theory	83
5.1.Objective and motivation	83
5.2.Introduction to analytical techniques	86
5.3.Details of materials	90
5.4.Propagation of THz through different types of composite systems	93
5.5.Result and discussion	95
5.5.1. Optical parameters of composites with negligible scattering	95
5.5.2. Optical parameters of composites with absorptive and dispersive fillers.....	103
5.6.Conclusion	115
6. Identification and quality control of Pharmaceuticals using THz-TDS	118
6.1.Objective and motivation	118
6.2.Materials and methods	120
6.3.Result and discussion	122
6.4.Conclusion	129

7. Application of THz spectroscopy and imaging for investigation of biological systems	131
.....	
7.1. Identification of phenotypes of <i>Arabidopsis thaliana</i> using THz-TDS	131
7.1.1. Objective and motivation	131
7.1.2. Materials and methods	133
7.1.3. Result and discussion	135
7.1.4. Conclusion	139
7.2. Identification of plant pigments using THz-TDS and Raman spectroscopy	139
7.2.1. Objective and motivation	139
7.2.2. Materials and methods	141
7.2.3. Result and discussion	143
7.2.4. Conclusion	146
7.3. Simulation of hollow-core metallic waveguides using THz-TDS	147
7.3.1. Objective and motivation	147
7.3.2. Theory	148
7.3.3. Result and discussion	150
7.3.4. Conclusion	152
8. Conclusion and future perspective	153
8.1. Conclusion	153
8.2. Future perspective	159
References	161

List of figures

1.1. Schematic showing the timeline of major developments in the field of THz technology. The picture has been adapted from Lewis [7]. In this figure, yellow boxes represent THz detectors, green boxes represent analytical techniques, orange boxes represent THz sources and blue boxes represent developments related to the optoelectronic techniques of THz generation and detection	2
1.2. THz band in the EM wave spectrum showing its typical range	3
1.3. Some of the characteristics of the THz radiation (left) and critical application areas of the THz band (right)	4
1.4. The energy levels present in a diatomic molecule. The actual spacing between the energy levels is different from the pictorial representation in the above figure. The actual spacing between electronic levels is much larger than the shown spacing and the actual spacing between the rotational levels is much smaller than the shown spacing	7
1.5. A simple illustration of the harmonic model of a one-dimensional ionic crystal showing the normal lattice mode in the crystal. In the figure, $u_{\pm,n}$ represents the displacement of ions with respect to the equilibrium coordinate of the n^{th} unit cell, $k_{1,2}$ are the spring constants related to the two bonds, a is lattice constant and d is bond length	8
1.6. Flowchart showing an overview of the dissertation	12
2.1. Schematic showing the classification of THz sources based on their generation technique discussed in this chapter. The techniques underlined are used for most of the experimental work in the subsequent chapters	15
2.2. Schematic showing the lasing frequency and power of the generated THz radiation using some of the common molecular lasers	18

2.3.	A comparison between interband and intersubband transition in semiconductor quantum well structure	19
2.4.	(a) Visual image of typical THz QCL (b) band structure and electron wave function moduli squared of a single-mode bound-to-continuum THz QCL and (c) scanning electron microscopy (SEM) and transmission electron microscopy (TEM) images of a mid-infrared QCL. The picture was taken from Rakic <i>et al.</i>	20
2.5.	(a) Schematic showing the generation of THz pulse from a photoconductive antenna excited by a femtosecond laser pulse and (b) side view of the photoconductive antenna with hemispherical silicon lens used for controlling the divergence of the generated THz radiation.....	22
2.6.	Schematic representation of different types of THz detectors discussed in this chapter. The type of detector underlined has been employed in subsequent chapters for the experimental work	24
2.7.	(a) Schematic showing detection of THz radiation using a photoconductive detector and (b) the THz sampling using the optical probe (the red pulse is the THz pulse and the blue Gaussian pulses are the optical probe pulse).....	27
2.8.	Schematic of PCA based THz-TDS system in transmission mode. The area shown inside the red dashed box shows the free-space propagation of THz radiation and the alignment of the PCAs and OAPMs can be changed to change the mode of operation from transmission to reflection and vice-versa	29
2.9.	Schematic showing free space propagation of THz radiation in a PCA-based THz-TDS setup in (a) transmission and (b) reflection configuration. In the above figure, the red arrow indicates optical fiber and the blue arrow indicates electrical cables connected to the PCAs.....	30

2.10. THz time-domain waveform of air at 40 % (cyan) and 6 % (red) humidity level and corresponding frequency domain response (amplitude and phase) obtained by taking the FFT. The inset in the time-domain plot shows the zoomed-out THz pulse. The sharp absorption lines in the amplitude plot indicate the water vapour absorption lines present in the environment and the intensity of the absorption lines changes with the amount of water vapour present in the free space path.....	31
2.11. Schematic of THz QCL based laser feedback interferometry imaging setup showing different modes of operation	32
2.12. Schematic of the designed Raman spectroscopy system consists of three lasers (532, 491.7 & 561.4 nm); here, green and blue lines represent the path of excitation laser beams, and red arrows show the direction of scattered light. Nomenclature: M - mirror, L - lens, S – manual-slit, BE- beam expander, MO - microscope objective, BPF - BraggGrate™ Bandpass filter, BBS - BraggGrate™ Beam splitter, BNF - BraggGrate™ Notch filter, EF – edge filter, and f (in bracket) is used for the optical components mounted on the flippers or flip platform. The figure is taken from Garg <i>et al.</i> [.....	34
2.13. Raman spectrum of Sulfur acquired with three different excitation wavelengths. Laser power was set at 20 mW with a slit width of 50 μm	35
3.1. Absorption coefficient of water at 20 °C in the THz region and the mid-infrared region. The picture depicts that the absorption is contributed by the translational and rotational modes of water. This representation has been adapted from Zhang <i>et. al</i>	39
3.2. Theoretical model of leaf heterostructure showing the internal parts of the leaf, which also includes air gaps and the water inside the leaf	41
3.3. Pictorial representation of the interaction of THz radiation with leaf in transmission (left) and reflection (right) configuration	42

3.4. (a) broadband time domain response of DI water and (b) corresponding amplitude spectrum obtained by converting the time domain signal to the frequency domain. The refractive index (c) and absorption coefficient (d) have been extracted from the phase and the amplitude spectrum respectively	45
3.5. Variation of time domain THz response of bamboo, mango and devil's ivy leaves with respect to time from the sample collection. The reference signal is of air as it is offering minimum absorption and dispersion of the THz signal.....	46
3.6. Variation of absorption coefficient and relative water content present in the leaf samples at different detection times. The calculations have been done considering DI water as the reference that represents 100 % water content	48
3.7. Frequency-dependent amplitude spectrum of bamboo, mango and devil's ivy leaf extracted by taking FFT of the time domain response at different time instances. The black curve in the three plots represents the amplitude spectrum of air (a common reference to all the samples).....	49
3.8. Absorbance response of bamboo, mango and devil's ivy leaf at two different frequencies, that is, 1.0 and 2.55 THz with respect to time from leaf plucking	50
3.9. Time domain waveform and the spectroscopic signal obtained from freshly plucked leaf and its reference (left) and FFT of the image and spectroscopic signal (right)	52
3.10. Amplitude and phase images of leaf 1 acquired after 30 minutes (T1), 180 minutes (T2) and 360 minutes (T3) from plucking extracted at different frequency points.....	53
3.11. Amplitude and phase images of leaf 2 acquired after 30 minutes (T1), 180 minutes (T2) and 360 minutes (T3) from plucking extracted at different frequency points.....	54
3.12. Spatial and temporal variation of reflected THz amplitude from the two leaves extracted from the images acquired after 30 minutes, 24 hours and 48 hours of plucking	56

3.13. Schematic showing the post-processing of experimental data: Typical experimentally obtained SM signal using THz QCL LFI imaging setup and the post-processed amplitude and phase images	58
3.14. Amplitude and phase images of two leaves from each plant sample obtained in water-stressed condition (T1) and after 1 (T2), 2 (T3) and 3 (T4) hours from the time it was watered	59
4.1. Schematic showing propagation of THz radiation in free space and interaction with sample in THz-TDS setup (left) and schematic of ULF-RS setup (right)	67
4.2. Flow chart (left panel) and pictorial representation (right panel) of the steps involved in pellet preparation using hydraulic pellet press	68
4.3. Calibration curve between sample mass and pellet thickness which indicates that the thickness of sample is directly proportional to the sample mass	69
4.4. THz time-domain (left) and frequency-domain (right) response of dry air showing the maximum usable frequency of the system recorded for air	69
4.5. Visual images of samples in pellet form (for THz-TDS study) and powder samples (for ULF-RS study) and their classification	70
4.6. Molecular structure and spectral responses of aromatic nitro-compounds obtained using THz-TDS (second panel) and ULF Raman (third panel with Stokes and anti-Stokes lines in the inset). Arrows of different colour are used to differentiate between the observed resonant modes. Peaks common to the class are indicated with black arrow; orange arrow is used to highlight the common peaks of Nitrotoluenes subclass and red arrow points the common peaks for the isomers of Dinitrotoluenes).....	73
4.7. The dotted line shows the intramolecular hydrogen bonds in nitrotoluenes which lead to twisting of NO ₂ group in the molecules	74

4.8.	Molecular structure and spectral responses of derivatives of benzoic acids obtained using THz-TDS (second panel) and ULF Raman (third panel with Stokes and anti-Stokes lines in the inset). Arrows of different colour are used to differentiate between the observed resonant modes. Peaks common to the class are indicated with black arrow and red arrow points the common peaks for the isomers of NBA.....	75
4.9.	Pictorial representation of intermolecular interaction in isomers of NBA. Black dotted lines represent hydrogen bonding between carboxyl groups which forms dimer of the compounds and cyan dotted lines represent other intermolecular hydrogen bonds.....	77
4.10.	Pictorial representation of low energy normal vibrational modes presents in potassium nitrate molecule.	78
4.11.	Molecular structure and spectral responses of derivatives of benzoic acids obtained using THz-TDS (second panel) and ULF Raman (third panel with Stokes and anti-Stokes lines in the inset). The peaks observed are indicated by arrow in the spectrum	79
5.1.	Representation of typical incident THz signal (black curve) and transmitted sample (red curve) in time-domain (left panel) and frequency domain (right panel)	87
5.2.	(a) Visual images of the standalone pellets and (b) visual images of composite pellets with detailed description variations in filler concentration and sample weight	92
5.3.	Variation of thickness of compressed pellets with respect to the total weight of sample used to prepare the corresponding pellet. Teflon has the highest compression factor while PE has the lowest compression strength	93
5.4.	Schematic representing the distribution of particles, particle shape and size of lactose (top) and MCC (bottom) pellets and their effect on the propagation of THz radiation through the two media. In the figure, t_0 represent incident THz radiation and t_1 , t_2 and t_3 represent the pulse position of transmitted THz radiation.....	94

5.5.	Frequency spectrum of composite pellets with different volume fraction of 2,6 DNT with purging at 2000 averages (top left), without purging with 6 averages (bottom left), 4 NT with purging at 2000 averages (top right) and without purging with 6 averages (bottom right) as guest in PE matrix	96
5.6.	Frequency dependent amplitude and phase images of 4 NT-PE and 2,6 DNT-PE composite series with different volume fraction of filler material	98
5.7.	Extracted effective permittivity (real and imaginary part) of 2,6 DNT-PE composites using BL, M-G, PvS and LLL approach at 1 THz and 3 THz	101
5.8.	Extracted effective permittivity (real part in left and imaginary part in right) of 4 NT-PE composites using BL, M-G, PvS and LLL approach at 1 THz and 3 THz	102
5.9.	(a) Microscopic images of the samples in powder form clearly showing the particle shape and the average particle size of Lactose (75 micron), MCC (40 micron), PE (40 micron) and Teflon (20 micron) and (b) plot showing the amount of porosity present in the pellets of four samples with different sample weight. The dotted line corresponds to the mean value of porosity concentration.	104
5.10.	(a) THz time-domain response of the samples for constant sample weight of 850 mg and (b) corresponding frequency spectrum obtained by taking the FFT of the time-domain signal (the arrow shows the usable bandwidth range of MCC and lactose).....	105
5.11.	Complex refractive indices of Teflon and PE, both polymers, given in the left panel and pure lactose and MCC, used as fillers, shown in right panel. The plots are with double y-axis, the refractive index is shown on the left y-axis with solid lines and the extinction coefficient is represented on the right y-axis with dashed lines.....	106
5.12.	Volume fraction of constituent material of composites, that is, polymer, filler and air-pores at different concentrations	108

5.13. THz amplitude and phase images of ternary composite extracted for different concentration of guest material. The bio-fillers, lactose and MCC, are used as guest and PE and Teflon as polymer host. The images were extracted at different frequencies including the phonon resonant absorption lines of lactose at 0.53, 1.19, 1.38, 1.82 and 2.45 THz and one non-resonant frequency line at 0.90 THz (highlighted with dashed box). The system dynamic range is more than 90 dB at 0.9 THz.	109
5.14. Variation of transmittance (%) and pulse width of the THz signal through different composite pellets with different inclusion concentrations	110
5.15. Surface plots showing the effective refractive index and extinction coefficient of the four composite compounds over the frequency range of 0.2 – 4. The plots also show the THz response of the composites with different concentration of filler material extracted using numerical method and LLL EMT approach.....	112
5.16. Surface plots illustrating the variation trend of refractive index (top) and extinction coefficient (bottom) the ternary composites (air-filler-polymer, air is present in all composite hence not mentioned separately) with respect to the filler concentration and thickness of the samples. The complex refractive indices have been extracted using the BL model and LLL model at 0.9 THz.....	114
5.17. Surface plots illustrating the variation trend of refractive index (top) and extinction coefficient (bottom) the ternary composites (air-filler-polymer, air is present in all composite hence not mentioned separately) with respect to the filler concentration and thickness of the samples. The complex refractive indices have been extracted using the BL model and LLL model at 2.55 THz.....	115
6.1. Visual images of the pharmaceutical drugs investigated in this chapter	121

6.2. Absorption spectrum of lactose (left panel), the resonant absorption peaks have been indicated with green arrows in the plot and the molecular structure of lactose has been shown in the right panel	122
6.3. Spectral response of Losar*-H and lactose in the left panel and Amlosafe-AT (1:1 wt. ratio with Teflon) in the right panel. The purple arrow represents the resonant peaks of IPI and the red arrow indicates the absorption modes of API.....	123
6.4. Frequency spectrum of Nitrocontin®, Sorbitrate® and Monotrate®. The spectra were acquired for different concentrations of drugs mixed in Teflon	124
6.5. 3D ball and stick molecular structure of nitroglycerin, isosorbide dinitrate and isosorbide mononitrate, the three APIs of pharmaceutical drugs	126
6.6. (a) Frequency spectra, (b) absorption spectra of the investigated pharmaceuticals and lactose pure (IPI) pellet and (c) molecular structures of the active pharmaceutical ingredients present in the formulated tablets.....	127
6.7. Effective refractive index (left panel) and absorption coefficient (right panel) of the pharmaceuticals extracted using the BL model.....	128
7.1. Visual images and microscopic images showing different stages of <i>Arabidopsis thaliana</i>	134
7.2. Visual images of day 5 and day 12 <i>Arabidopsis thaliana</i> of Col. type and two mutants.	134
7.3. Spectral response of different parts of 5 days and 12 days old phenotypes of <i>Arabidopsis thaliana</i> using THz-TDS	135
7.4. Microscopic images of different parts of 5 days and 12 days old phenotypes of <i>Arabidopsis thaliana</i> (with a magnification of 20X).	137

7.5. THz amplitude images of the three phenotypes of 12 days old <i>Arabidopsis thaliana</i> . The images are frequency deconvoluted images at different frequencies	138
7.6. Microscopic images showing the formation of fungal infection on the plants	138
7.7. Molecular structure of (a) chlorophyll (b) β -carotene (c) betalain and (d) anthocyanin	142
7.8. Visual images of the pigments in ethanol solution and pellet form and systematic procedure used here for the extraction of powdered chlorophyll	143
7.9. (a) Raman spectra of plant pigments extracted in ethanol solution. The peaks values corresponding to the pigments mentioned in the plots; the peaks corresponding to the vibrational modes of ethanol has been highlighted with grey band and (b) Raman spectrum of chlorophyll in powder form (all peaks correspond to chlorophyll).....	144
7.10. THz spectra of chlorophyll, betalain, β -carotene and anthocyanin for different concentrations of pigment: Teflon pellets	145
7.11. (a) Schematic of the proposed hybrid-cladding model and (b) flow-chart showing the systematic procedure employed for simulation of the proposed model in COMSOL Multiphysics	150
7.12. Surface plots showing the modal analysis of hybrid-cladding hollow-core metallic waveguide at different frequencies	150
7.13. Real and imaginary part of effective mode index of the waveguide (in left panel) and the attenuation loss of the structure with respect to frequency (in the right panel)	151
8.1. Schematic showing the overview of the major findings of the dissertation. The chapters are colour coded and the staircase arrangement of the boxes corresponding to chapter 7 has been used for an easy and clear representation of the conclusions of different sections of the chapter	158

List of tables

3.1. System parameters used for image acquisition in the PCA based and QCL LFI based THz imaging techniques	43
3.2. The calculated value of SNR at the frequencies of interest and corresponding absorption coefficient of liquid water.	52
4.1. Low energy spectral fingerprints of chemicals obtained using THz-TDS and ULF-RS in this study reported in this study. The observed peaks are compared with the peaks reported in literature corresponding to the reference in square bracket. The peaks with dagger (†) symbol are observed using both the techniques. Under a specific spectroscopic platform, peaks in bold represent class selective spectral features; peaks in orange bold represent common spectral features of a subclass of chemicals; peaks in red bold represent common spectral features of isomers of a chemical; peaks in <i>blue bold italics</i> represent strong unique features for a chemical for spectral identification	80
5.1. Physical properties of polymers and filler materials used in the study	90
5.2. Summary of the materials optical characteristics at 1 THz using numerical model and the most suitable EMT model	107
6.1. Detail of pharmaceutical drugs investigated in this dissertation	121
6.2. Mode assignment of peaks observed for pure lactose.	123
6.3. Peaks observed for different drugs in this study and the previously reported peaks of APIs from theoretical calculations	127
7.1. Peaks observed and the sample specifications for which the peaks were observed using THz-TDS and Raman spectroscopy	146

List of abbreviations

1. THz : Terahertz
2. EM : Electromagnetic
3. TDS : Time-domain spectroscopy
4. IC : Integrated circuits
5. QCL : Quantum cascade lasers
6. LFI : Laser feedback interferometry
7. BWO : Backward wave oscillators
8. FEL : Free electron lasers
9. TEM : Transmission electron microscopy
10. SEM : Scanning electron microscopy
11. MBE : Molecular beam epitaxy
12. OR : Optical rectification
13. fs : Femtosecond
14. NL : Non-linear
15. PCA : Photoconductive antenna
16. EO : Electro-optic
17. MLHS : Multi-layered heterostructure
18. LT : Low temperature
19. SM : Self mixing
20. ULF-RS : Ultra-low frequency Raman spectroscopy
21. SLM : Single longitudinal mode
22. VHF : Volume holographic filters
23. CCD : Charge-coupled detectors
24. HPBF : Holographic bandpass filters

- 25. MO : Microscope objective
- 26. BNF : BraggGrate notch Filter
- 27. BBS : BraggGrate beam splitter
- 28. BPF : BraggGrate bandpass filters
- 29. EF : Edge filter
- 30. DI : Deionized
- 31. SNR : Signal-to-noise ratio
- 32. FFT : Fast Fourier transform
- 33. FTIR : Fourier transform infrared spectroscopy
- 34. RS : Raman spectroscopy
- 35. API : Active pharmaceutical ingredients
- 36. EMT : Effective medium theory
- 37. BL : Beer-Lamberts'
- 38. M-G : Maxwell-Garnet
- 39. PvS : Polder van Santen
- 40. LLL : Landau Lifshitz Looyenga
- 41. FWHM : Full width at half maxima
- 42. MCC : Microcrystalline cellulose
- 43. PSD : Particle size distribution
- 44. PE : Polyethylene
- 45. IPI : Inactive pharmaceutical ingredient
- 46. PAT : Process analytical technology
- 47. NG : Nitroglycerine
- 48. ISDN : Isosorbide dinitrate
- 49. ISMN : Isosorbide mononitrate

- 50. FDA : Food and drugs administration
- 51. GM : Genetically modified
- 52. ISAAA : International service for accusation of agri-biotech applications
- 53. PCR : Polymerase chain reaction
- 54. ELISA : Enzyme-linked immune sorbent assay
- 55. SVM : Support vector machine
- 56. WC : Water content
- 57. DSSC : Dye-sensitized solar cells
- 58. TE : Transverse electric
- 59. TM : Transverse magnetic
- 60. ITO : Indium tin oxide
- 61. GZO : Gallium doped zinc oxide